

Error estimation and uncertainty quantification for first time to a threshold value

Jehanzeb H. Chaudhry, Donald Estep, Zachary Stevens and Simon J. Tavener

November 11, 2021

Abstract

Classical *a posteriori* error analysis for differential equations quantifies the error in a Quantity of Interest (QoI) which is represented as a bounded linear functional of the solution. In this work we consider *a posteriori* error estimates of a quantity of interest that cannot be represented in this fashion, namely the time at which a threshold is crossed for the first time. We derive two representations for such errors and use an adjoint-based *a posteriori* approach to estimate unknown terms that appear in our representation. The first representation is based on linearizations using Taylor's Theorem. The second representation is obtained by implementing standard root-finding techniques. We provide several examples which demonstrate the accuracy of the methods. We then embed these error estimates within a framework to provide error bounds on a cumulative distribution function when parameters of the differential equations are uncertain.

1 Introduction

There are many situations in which the purpose of a computation is to determine *when* a functional of the solution to (1) achieves a certain event, for example when a temperature or a species concentration reaches a specified level, the wave height of a tsunami crosses a threshold at a certain location, an orbiting body completes a revolution etc. In this article we perform *a posteriori* analysis for the error in the computed value and computed probability distribution of the time at which a threshold value is realized for the first time in the context of ordinary differential equations (ODEs). More precisely, consider a system of first order ODEs

$$\dot{y} = f(y, t; \theta), \quad t \in (0, T], \quad y(0) = y_0, \quad (1)$$

where $\dot{y} \equiv \frac{dy(t)}{dt}$, $f : \mathbb{R}^m \times \mathbb{R} \rightarrow \mathbb{R}^m$ is a Lipschitz continuous function and θ is a deterministic or random parameter. Let $S(y(t))$ be a linear functional of $y(t)$ and $Q(y)$ be the first time $t \in (0, T]$ at which a threshold $S(y(t)) \geq R$ is crossed. That is,

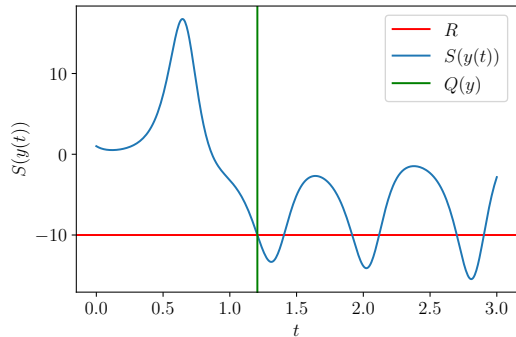
$$Q(y) := \min_{t \in (0, T]} \arg(S(y(t)) = R). \quad (2)$$

Hence, we refer to this as a non-standard QoI in the context of *a posteriori* error analysis.

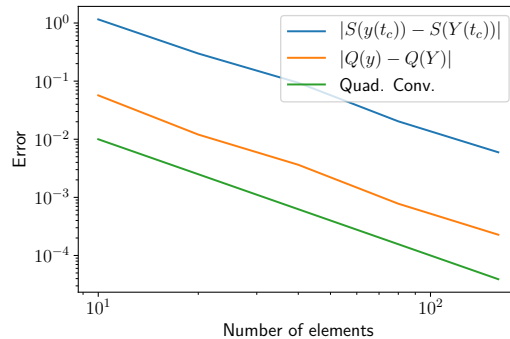
Example: Lorenz System To illustrate the QoI (2), we consider the Lorenz system,

$$\left. \begin{aligned} \dot{y}_1 &= \sigma(y_2 - y_1), \\ \dot{y}_2 &= ry_1 - y_2 - y_1y_3, \\ \dot{y}_3 &= y_1y_2 - by_3, \end{aligned} \right\} t \in (0, 3] \quad \text{with} \quad \left\{ \begin{aligned} y_1(0) &= 1, \\ y_2(0) &= 0, \\ y_3(0) &= 24. \end{aligned} \right. \quad (3)$$

with $\sigma = 10$, $r = 28$, and $b = \frac{8}{3}$ (see §4.2 for more details of this example). We define the functional $S(y(t)) = y_1(t)$ and set the threshold value $R = -10$. Figure 1a illustrates an accurate reference



(a) Reference solution and QoI for Lorenz system.



(b) Converge rates of the error in QoI and the error in the functional. Here, y and $Q(y) \equiv t_t$ are the true solution and QoI. The numerical solution and QoI, Y and $Q(Y) \equiv t_c$, are computed using the cG(1) method with different numbers of elements.

Figure 1

solution as well as the threshold value and the QoI. Figure 1b shows the convergence rates for the error in the functional at a numerically computed QoI and the error in the QoI itself.

Standard adjoint-based *a posteriori* error analysis seeks to estimate the error in a quantity of interest (QoI) that can be expressed as a bounded functional of the solution and is widely used for a host of numerical methods [1, 4, 6–12, 14, 16–19, 22, 23, 29, 31, 33, 35, 36, 39, 41]. In these cases, the error analysis involves computable residuals of the numerical solution, the generalized Green’s function solving an adjoint problem and variational analysis [1, 7, 32, 35, 36]. This work is briefly summarized for initial value problems in §2.1. It is usually employed within a finite element (variational) solution strategy, but can also be applied to finite difference and finite volume methods by recasting them as equivalent finite element methods [15, 20, 21, 24, 26, 27, 30, 34, 42]. Nonlinear QoIs are treated by first linearizing around a computed solution e.g. see [9].

The goal of the current work is to derive accurate error estimates for the non-standard QoI (2) that *cannot* be expressed as a bounded linear functional of the solution y . In addition, we use the result to bound the error in an empirical distribution function for the nonstandard QoI corresponding to a stochastic parameter θ . This is similar to the *a posteriori* analysis for the error in CDF for standard QoIs for PDEs with random coefficients and random geometries is carried out in [13, 37, 38].

The analysis for the error in the non-standard QoI appears in §2. The first approach in §2.2 takes advantage of linearization via Taylor series and employs auxiliary quantities of interest to obtain a formula that directly estimates the error in the QoI. Our second approach, in §2.3 proceeds by using different root finding methods and again employs auxiliary quantities of interest. Numerical results supporting the accuracy of the error estimates for a deterministic system appear in §3. Details of the error estimate for the CDF are provided in §2.5 and the bounds are computed for several examples in §4.

2 *A posteriori* error analysis

For simplicity, we consider a continuous FEM approximation $Y(t)$, $t \in [0, T]$ for data $y(t)$, with approximate functional $S(Y(t))$ as illustrated in Figure 2. For each problem the linear functional $S(y(t))$ and the value of R are specified, and the problems are solved using two different numerical schemes: (i) variational cG(1) finite element scheme using 40 equally-sized elements and high-order Gaussian quadrature, and (ii) Crank-Nicolson finite difference scheme with 21 equally-spaced nodes.

However, we stress that the analysis can be extended to a wide variety of numerical methods for equivalence to a finite element method can be established. Finite difference schemes for which a posteriori error estimates have been derived include explicit schemes, IMEX methods, BDF, Runge-Kutta, Lax-Wendroff, multirate and parallel-in-time methods [15, 17, 20, 21, 24, 26, 27, 30, 34, 42].

Given the partition $\tau = \{0 = t_0, t_1, \dots, t_N = T\}$ define the space,

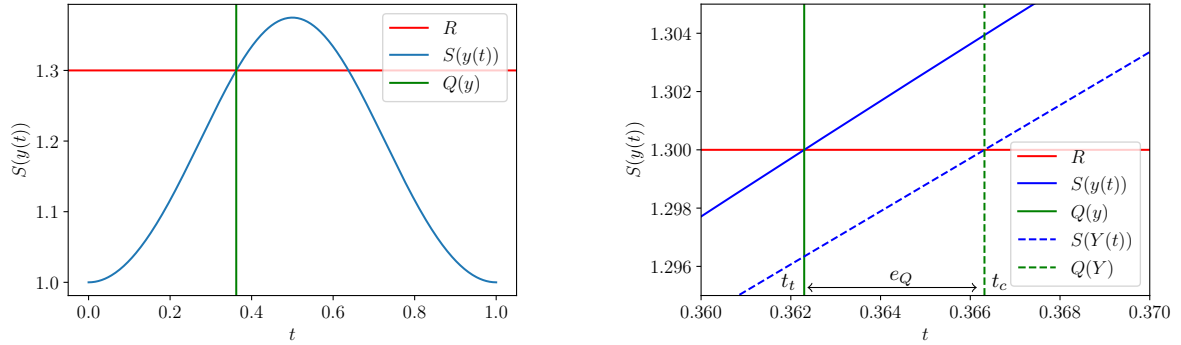
$$\mathcal{V}^q = \{w \in C^0([0, T]; \mathbb{R}^m) : w|_{I_n} \in \mathcal{P}^q(I_n), 1 \leq n \leq N\},$$

where $\mathcal{P}^q(I_n)$ is the space of all polynomials of degree q or less on $I_n := [t_n, t_{n+1}]$. The continuous Galerkin finite element method of order $q + 1$, denoted cG(q), for solving (1) is defined interval-wise by: Find $Y \in \mathcal{V}^q$ such that

$$\int_{t_n}^{t_{n+1}} \dot{Y}(t) \cdot v(t) dt = \int_{t_n}^{t_{n+1}} f(Y, t) \cdot v(t) dt, \quad \forall v \in \mathcal{P}^{q-1}(I_n), \quad (4)$$

for $n = 0, 1, 2, \dots, N - 1$. The cG(q) schemes are variational and hence well suited for adjoint based analysis. However, the Crank-Nicolson is also nodally equivalent to a variational scheme, see Theorem 4 in Appendix A.

In Sections 2.1, 2.2 and 2.3 it is assumed that θ assumes a fixed value and is omitted from being written explicitly. The role of θ is considered in §2.5.



(a) Graph showing true functional $S(y(t))$, chosen value of R , and true value of QoI for the example in §3.1.

(b) Close up of true QoI and numerical QoI for the example in §3.1, solved using the Crank-Nicolson scheme.

Figure 2

For a given constant R , define t_t and t_c such that

$$S(y(t_t)) = R = S(Y(t_c)) \quad (5)$$

where $t_t = Q(y)$ is the true value of the QoI, and $t_c = \min_{t \in (0, T]} \arg(S(Y(t)) = R)$ is a computed approximation to the QoI. Define the true error in the QoI, e_Q , to be

$$e_Q = t_t - t_c. \quad (6)$$

The aim is to derive an accurate error estimate $\eta \approx e_Q$. The accuracy of the error estimate is quantified by the effectivity ratio,

$$\rho_{\text{eff}} = \frac{\eta}{e_Q}. \quad (7)$$

An effectivity ratio close to one indicates an accurate error estimate.

Also let ϵ denote the error in the solution to (1), i.e.,

$$\epsilon(t) = y(t) - Y(t). \quad (8)$$

2.1 Adjoint-based *a posteriori* error analysis for standard QoIs

We derive error estimates for the nonstandard QoI in terms of expressions involving errors in linear functionals of the numerical solution. This section presents a standard *a posteriori* error estimate for a linear functional of a solution. Let (\cdot, \cdot) denote the inner-product pairing in \mathbb{R}^n .

Theorem 1 (Adjoint-based *a posteriori* error analysis for IVPs). *Given a finite element solution $Y(t)$ of (1) and $\psi \in \mathbb{R}^n$, the error $(\psi, \epsilon(\hat{t}))$ at $\hat{t} \in (0, T]$ is represented as*

$$(\psi, \epsilon(\hat{t})) = (\psi, y(\hat{t})) - (\psi, Y(\hat{t})) = \int_0^{\hat{t}} (\phi, [f(Y, t) - \dot{Y}]) dt, \quad (9)$$

where ϕ is the solution to the adjoint equation

$$\begin{cases} -\dot{\phi} = \overline{f_{y,Y}(t)}^T \phi, & t \in [\hat{t}, 0], \\ \phi(\hat{t}) = \psi, \end{cases} \quad (10)$$

with

$$\overline{f_{y,Y}(t)} = \int_0^1 \frac{df}{dz}(z, t) ds \quad (11)$$

and $z = sy + (1-s)Y$,

Proof. The proof is standard see [29]. \square

2.2 *A posteriori* analysis for the non-standard QoI based on Taylor series

Theorem 2. *For an approximate solution $Y(t)$ to (1) and a bounded linear functional $S(y(t))$ on $(H^1((0, T]))^n$, the error in the QoI (2) is given by*

$$t_t - t_c = \frac{S(Y(t_c)) - S(y(t_c)) - \mathcal{R}_1(t_c, t_t)}{\frac{\partial S}{\partial t}(y(t_c) + \nabla_y S(Y(t_c)) \cdot f(Y, t_c) + \nabla_y [\nabla_y S(Y(t_c)) \cdot f(Y, t_c)] \cdot (y(t_c) - Y(t_c)) + \mathcal{R}_2(Y(t_c))}}, \quad (12)$$

where the remainder terms $\mathcal{R}_1(t_t, t_c)$ and $\mathcal{R}_2(t_c)$ satisfy

$$\mathcal{R}_1(t_t, t_c) = \frac{1}{2} \frac{d^2 S}{dt^2}(y(\xi))(t_t - t_c)^2,$$

for some ξ between t_t and t_c and

$$\mathcal{R}_2(Y(t_c)) = \|y(t_c) - Y(t_c)\| \mathcal{H}_2(Y(t_c)), \text{ for } \mathcal{H}_2 \text{ with } \lim_{Y(t_c) \rightarrow y(t_c)} \mathcal{H}_2(Y(t_c)) = 0,$$

and $\|\cdot\|$ denotes the Euclidean norm on \mathbb{R}^n .

Proof. From the definition of the functional $S(y(t))$ and R ,

$$S(Y(t_c)) = R = S(y(t_t)). \quad (13)$$

Expanding $S(y(t_t))$ using Taylor's Theorem with remainder centered at t_c (e.g. see [2]) in (13),

$$S(Y(t_c)) = S(y(t_c)) + \frac{dS}{dt}(y(t_c))(t_t - t_c) + \mathcal{R}_1(t_c, t_t), \quad (14)$$

Applying the chain-rule to the derivative in (14) and using (1) gives

$$S(Y(t_c)) = S(y(t_c)) + \left[\nabla_y S(y(t_c)) \cdot f(y, t_c) + \frac{\partial S}{\partial t}(y(t_c)) \right] (t_t - t_c) + \mathcal{R}_1(t_c, t_t).$$

Adding and subtracting the term $\nabla_y S(Y(t_c)) \cdot f(Y, t_c)$ inside the square brackets gives

$$\begin{aligned} S(Y(t_c)) &= S(y(t_c)) \\ &+ \left[\nabla_y S(Y(t_c)) \cdot f(Y, t_c) + (\nabla_y S(y(t_c)) \cdot f(y, t_c) - \nabla_y S(Y(t_c)) \cdot f(Y, t_c)) + \frac{\partial S}{\partial t}(y(t_c)) \right] (t_t - t_c) \\ &+ \mathcal{R}_1(t_c, t_t). \end{aligned} \quad (15)$$

Using the multi-variable Taylor's Theorem with remainder centered at Y (e.g. see [3]) gives

$$\nabla_y S(y(t_c)) \cdot f(y, t_c) - \nabla_y S(Y(t_c)) \cdot f(Y, t_c) = \nabla_y [\nabla_y S(Y(t_c)) \cdot f(Y, t_c)] \cdot (y(t_c) - Y(t_c)) + \mathcal{R}_2(Y(t_c)), \quad (16)$$

where the remainder is of the form

$$\mathcal{R}_2(Y(t_c)) = \frac{1}{2} (Y(t_c) - y(t_c))^\top \mathbf{H}_y (\nabla_y S(\xi) \cdot f(\xi, t_c)) (Y(t_c) - y(t_c)), \quad (17)$$

for some ξ between $y(t_c)$ and $Y(t_c)$, and where \mathbf{H}_y is the Hessian

$$(\mathbf{H}_y)_{i,j} = \frac{\partial^2}{\partial y_i \partial y_j}.$$

Substituting (16) in to (15) and rearranging to isolate the error of the QoI, results in

$$\begin{aligned} (t_t - t_c) &= \\ &\frac{S(Y(t_c)) - S(y(t_c)) - \mathcal{R}_1(t_c, t_t)}{\frac{\partial S}{\partial t}(y(t_c)) + \nabla_y S(Y(t_c)) \cdot f(Y, t_c) + \nabla_y [\nabla_y S(Y(t_c)) \cdot f(Y, t_c)] \cdot (y(t_c) - Y(t_c)) + \mathcal{R}_2(Y(t_c))}. \end{aligned} \quad (18)$$

□

We denote the error in the non-standard QoI as $e_Q = t_t - t_c$.

Corollary 1. *For functionals $S(y(t))$ that are independent of t ,*

$$e_Q = \frac{S(Y(t_c)) - S(y(t_c)) - \mathcal{R}_1(t_c, t_t)}{\nabla_y S(Y(t_c)) \cdot f(Y, t_c) + \nabla_y [\nabla_y S(Y(t_c)) \cdot f(Y, t_c)] \cdot (y(t_c) - Y(t_c)) + \mathcal{R}_2(Y(t_c))}. \quad (19)$$

Note that functionals $S(y(t))$ that depend directly on t require special treatment of the term $\frac{\partial S}{\partial t}(y(t_c))$ in (12). More precisely, one can use another application of Taylor's Theorem centered at $Y(t_c)$ in order to make this term computable.

Corollary 2. *For functionals of the form $S(y(t)) = v \cdot y(t)$, for some $v \in \mathbb{R}^n$, $\nabla_y S(y(t)) = v$, and (19) becomes*

$$\begin{aligned} e_Q &= \frac{-v \cdot (y(t_c) - Y(t_c)) - \mathcal{R}_1(t_c, t_t)}{v \cdot f(Y, t_c) + v^\top \nabla_y f(Y, t_c) \cdot (y(t_c) - Y(t_c)) + \mathcal{R}_2(Y(t_c))} \\ &= \frac{-v \cdot \epsilon(t_c) - \mathcal{R}_1(t_c, t_t)}{v \cdot f(Y, t_c) + v^\top \nabla_y f(Y, t_c) \cdot \epsilon(t_c) + \mathcal{R}_2(Y(t_c))} \end{aligned} \quad (20)$$

Obtaining a computable error estimate. Taylor's Theorem gives that the two functions \mathcal{R}_1 and \mathcal{R}_2 in equations (19) and (20) decay to zero super-linearly as $t_c \rightarrow t_t$ and $Y(t_c) \rightarrow y(t_c)$, respectively. Provided the numerical solution $Y(t)$ is fairly accurate, \mathcal{R}_1 will be small compared to the other terms in (14) and \mathcal{R}_2 will be small compared to the terms in (16). This leads to the first approximation of the error,

$$\eta(Y) = \frac{-v \cdot \epsilon(t_c)}{v \cdot f(Y, t_c) + (v^\top \nabla_y f(Y, t_c)) \cdot \epsilon(t_c)}. \quad (21)$$

Remark 1. Note that the functional S may achieve the value R at multiple times. Assume there exists a time $\hat{t} > t_t$ such that $S(y(\hat{t})) = R$. Equation (13) is then valid at time \hat{t} , i.e., $S(Y(t_c)) = R = y(\hat{t})$ and (12) follows with t_t replaced by \hat{t} and ξ replaced by $\hat{\xi}$. In the estimate (21) we approximate the term $\mathcal{R}_1(t_c, \cdot)$ by zero. If the numerical solution is sufficiently accurate, then $|t_t - t_c| < |\hat{t} - t_c|$ and $0 \approx \mathcal{R}_1(t_c, t_t) \ll \mathcal{R}_1(t_c, \hat{t})$. However, if the numerical solution is inaccurate, we may have the reverse situation, where $|t_t - t_c| > |\hat{t} - t_c|$, in which case the error estimate will be inaccurate or worse, $\mathcal{R}_1(t_c, \hat{t}) \approx 0$ and the estimate may indicate the value of $\hat{t} - t_c$ rather than $t_t - t_c$. We observe this phenomenon in §3.4.1 and is illustrated by Table 10 and Figure 6b.

The estimate (21) contains two terms that are linear functionals of the error at time t_c . These can both be approximated by the standard techniques in §2.1 as is discussed next.

First adjoint problem In order to estimate $-v \cdot \epsilon(t_c)$, we solve (10) with adjoint data $\psi = \psi_1 = -v$ and $\hat{t} = t_c$, then substitute the solution ϕ_1 in (9) to provide the estimate

$$\mathcal{E}_1(Y, \phi_1) \approx \psi_1 \cdot \epsilon(t_c) = -v \cdot \epsilon(t_c). \quad (22)$$

Second adjoint problem In order to estimate $v^T \nabla_y f(Y, t_c) \cdot \epsilon(t_c)$, we solve (10) with adjoint data $\psi = \psi_2 = v^T \nabla_y f(Y, t_c)$ and $\hat{t} = t_c$, then substitute the solution ϕ_2 in (9) to provide the estimate

$$\mathcal{E}_2(Y, \phi_2) \approx \psi_2 \cdot \epsilon(t_c) = v^T \nabla_y f(Y, t_c) \cdot \epsilon(t_c). \quad (23)$$

Computable error based on Taylor series and adjoint techniques. For an approximate solution $Y(t)$ to (1) and a linear functional $S(Y(t)) = v \cdot Y(t)$, a computable estimate of the error in the QoI (2) is obtained by substituting (22) and (23) in (21),

$$\eta(Y, \phi_1, \phi_2) = \frac{\mathcal{E}_1(Y, \phi_1)}{v \cdot f(Y, t_c) + \mathcal{E}_2(Y, \phi_2)}. \quad (24)$$

2.3 Error in non-standard QoI based on iterative techniques

Given an approximate solution $Y(t)$ to (1) with numerical QoI t_c , define $g(t)$ as

$$\begin{aligned} g(t) &= S(y(t)) - R, \\ &= S(Y(t)) + (S(y(t)) - S(Y(t))) - R, \end{aligned} \quad (25)$$

so

$$g(t_t) = 0. \quad (26)$$

In the case where $S(t)$ is a linear functional of $y(t)$, i.e., $S(y(t)) = v \cdot y(t)$, then

$$g(t) = S(Y(t)) + v \cdot \epsilon(t) - R.$$

At $t = \hat{t}$ we estimate $v \cdot \epsilon(\hat{t})$ by solving (10) with adjoint data $\psi = \psi_3 = v^T$ and substituting the solution ϕ_3 in to (9) to provide the estimate

$$\mathcal{E}_3(Y, \phi_3; \hat{t}) \approx v^T \cdot (y(\hat{t}) - Y(\hat{t})), \quad (27)$$

hence

$$g(\hat{t}) = S(Y(\hat{t})) + \mathcal{E}_3(Y, \phi_3; \hat{t}) - R.$$

We find t^* such that $g(t^*) \approx 0$ via a standard root finding procedure, then

$$\eta(Y) = t^* - t_c. \quad (28)$$

There are many options for root finding methods for computing η . In this article, we use two of the basic root finding methods: the secant method and the inverse quadratic method.

2.3.1 Error estimate based on the secant method

Given initial values x_0, x_1 , the method is defined by the recurrence

$$x_n = \frac{x_{n-2} * g(x_{n-1}) - x_{n-1} * g(x_{n-2})}{g(x_{n-1}) - g(x_{n-2})} \quad n = 2, 3, \dots \quad (29)$$

(See [40]). For the initial guesses the examples presented choose $x_0 < t_c < x_1$. These choices are made precise in the numerical examples in §3.

2.3.2 Error estimate based on inverse quadratic interpolation

Given initial values x_0, x_1, x_2 , the method is defined by the recurrence

$$x_n = \frac{x_{n-3} g_{n-2} g_{n-1}}{(g_{n-3} - g_{n-2})(g_{n-3} - g_{n-1})} + \frac{x_{n-2} g_{n-3} g_{n-1}}{(g_{n-2} - g_{n-3})(g_{n-2} - g_{n-1})} + \frac{x_{n-1} g_{n-2} g_{n-3}}{(g_{n-1} - g_{n-2})(g_{n-1} - g_{n-3})}. \quad n = 3, 4, \dots \quad (30)$$

(See [28]). The choice of the initial guesses is made precise in the numerical examples in §3.

2.4 Comparison of the two error estimation methods

The method based on Taylor series always requires fewer adjoint problems to be solved than using an iterative method. However, the estimate (21) neglects certain terms compared to the error representation (20). If any of the neglected terms are large, the error estimate may be inaccurate even though an accurate numerical solution is used. The iterative methods only rely on the initial guesses and point-wise error computation, which is computed accurately. The initial guesses defined in Section 3 surround the computed QoI, so as long as the computed solution is accurate enough the iterative methods will be accurate. Numerical comparisons of the two methods, as well as limitations of both are discussed throughout Section 3.

2.5 Error in a cumulative density function

If the differential equation (1) depends on a random parameter θ , then the solution $y(t; \theta)$ and the QoI, $Q(y; \theta)$, are random variables. As a random variable, $Q(y; \theta)$ has a corresponding cumulative distribution function (CDF):

$$P(t) = P(\{\theta : Q(y; \theta) \leq t\}). \quad (31)$$

An approximation to the CDF is computed using a finite number of approximate sample values $\{Q(Y^{[n]}, \theta^{[n]})\}_{n=1}^N$:

$$\hat{P}_N(t) = \frac{1}{N} \sum_{n=1}^N \mathbb{1}_{(-\infty, t]}(Q(Y^{[n]}, \theta^{[n]}) \leq t). \quad (32)$$

Where $\mathbb{1}_I$ is the indicator function over the interval I . A nominal sample distribution is computed using exact values of the QoI,

$$P_N(t) = \frac{1}{N} \sum_{n=1}^N \mathbb{1}_{(-\infty, t]}(Q(y^{[n]}, \theta^{[n]}) \leq t). \quad (33)$$

An estimate of the error in an approximate distribution of the QoI (2) is computed for three examples in §4. The estimate takes into account error contributions from stochastic sources that arise from finite sampling and deterministic sources that arise from the discretization of the ODE. The

computation utilizes the error estimate derived in §2.2. The expressions (32) and (33) allows us to decompose the error to isolate the stochastic and deterministic contributions:

$$P(t) - \hat{P}(t) = (P(t) - P_N(t)) + (P_N(t) - \hat{P}_N(t)). \quad (34)$$

This decomposition is used to derive the following error bound [13, 37, 38].

Theorem 3. For $0 < \varepsilon < 1$,

$$\left| P(t) - \hat{P}(t) \right| \leq \left(\frac{\hat{P}(t)(1 - \hat{P}(t))}{N\varepsilon} \right)^{1/2} + \frac{2}{N} \left| \sum_{n=1}^N \mathbb{1}_{[-|\eta^{[n]}|, |\eta^{[n]}|]} \left(t - Q(Y^{[n]}, \theta^{[n]}) \right) \right| + \frac{1}{2N\varepsilon}, \quad (35)$$

with probability greater than or equal to $1 - \varepsilon$, where $\eta^{[n]}$ is an error estimate for the QoI computed from the sample numerical solution.

The estimate (24) is used to compute $\eta^{[n]}$. The first term of (35) quantifies the error contribution from stochastic sources, while the second term represents error due to discretization.

3 Numerical examples

This section considers a wide range of types of linear and nonlinear ODEs in order to explore the accuracy of the estimates.

Since the Crank-Nicolson finite difference scheme is nodally equivalent to the cG(1) finite element method with a trapezoidal rule quadrature, given $t_i < t_c < t_{i+1}$, the numerical QoI may be computed by using linear interpolation as,

$$t_c = \frac{R(t_i - t_{i+1})}{Y(t_i) - Y(t_{i+1})} - \frac{t_i Y(t_i) - t_{i+1} Y(t_{i+1})}{Y(t_i) - Y(t_{i+1})}.$$

When implementing the secant method (29), the two grid-points closest to the QoI are used as initial guesses:

$$x_0 = t_L \text{ and } x_1 = t_R, \quad (36)$$

where $t_L < t_c < t_R$, with no other grid-points in between. For the inverse quadratic interpolation scheme (30), the initial guesses are the two closest grid-points to the left of the QoI and one to the right:

$$x_0 = t_{LL}, \ x_1 = t_L \text{ and } x_2 = t_R, \quad (37)$$

where $t_{LL} < t_L < t_c < t_R$, with no other grid-points in between. For most examples the adjoint solutions, needed for the estimates (22), (23) and (24), are computed using the cG(3) method with 100 finite elements, with the exceptions of §3.5 where cG(3) is used with 40 elements and §4.2 where cG(2) with 100 elements is used. For all methods define n_{adj} to be the number of adjoint solutions required to compute the error in the QoI. This number can be seen as the relative cost of implementing the different methods.

3.1 Linear problem

We consider the initial value problem

$$\dot{y} = \sin(2\pi t)y, \quad t \in (0, 1], \quad y(0) = 1,$$

with analytic solution

$$y(t) = \exp\left(\frac{1}{2\pi}(1 - \cos(2\pi t))\right).$$

Let $R = 1.3$ and $S(y(t)) = y(t)$. The true QoI is given by

$$t_t = Q(y) = \min_{t \in (0,1]} \arg(y(t) = 1.3) = \frac{1}{2\pi}(\arccos(-2\pi \ln(1.3) + 1)).$$

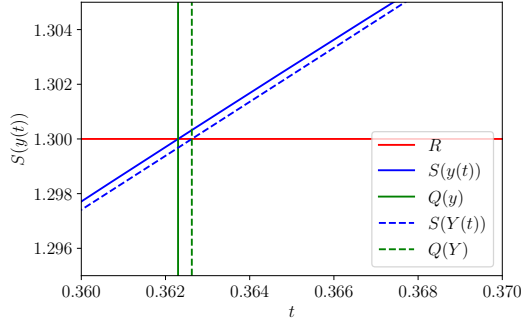
For this problem, the terms in (21) are

$$v = 1, f(y, t) = \sin(2\pi t)y, \nabla_y f(y, t) = \sin(2\pi t),$$

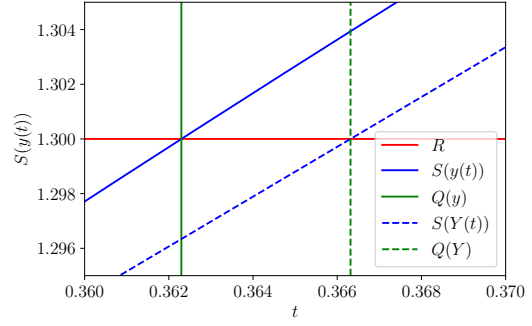
hence, for (22), (23), and (27) the values needed are

$$\psi_1 = -1, \psi_2 = \sin(2\pi t_c), \psi_3 = 1.$$

The true solution and QoI are shown in Figure 3. This graph includes a horizontal line at $S(y(t)) = R$, to indicate the threshold value of interest, as well as a vertical line denoting the true value of the QoI, i.e. the first time the threshold is crossed. Figure 3 compares the numerical QoI to the true value for both the numerical schemes. True errors, error estimates and effectivity ratios are provided in Tables 1 and 2. All methods provide excellent effectivity ratios, but the iterative methods require many more applications of Theorem 1 and hence require solving more adjoint problems of the form (10), as shown by the values of η_{adj} .



(a) Comparing cG(1) solution and computed QoI(2) to the true values for example in §3.1.



(b) Comparing Crank-Nicolson solution and computed QoI (2) to the true values for example in §3.1.

Figure 3

Method	t_c	t_{LL}	t_L	t_R	e_Q	η	ρ_{eff}	n_{adj}
Taylor series	0.3626	—	—	—	-3.267e-04	-3.269e-04	1.000	2
Secant	0.3626	—	0.35	0.375	-3.267e-04	-3.267e-04	1.000	6
Inverse quad.	0.3626	0.325	0.35	0.375	-3.267e-04	-3.267e-04	1.000	7

Table 1: Results of the different methods on the example in §3.1 using cG(1) with 40 elements.

Method	t_c	t_{LL}	t_L	t_R	e_Q	η	ρ_{eff}	n_{adj}
Taylor series	0.3663	—	—	—	-4.017e-03	-4.056e-03	1.010	2
Secant	0.3663	—	0.35	0.4	-4.017e-03	-4.017e-03	1.000	7
Inverse quad.	0.3663	0.3	0.35	0.4	-4.017e-03	-4.017e-03	1.000	7

Table 2: Results of the different methods on the example in §3.1 using Crank-Nicolson with 21 nodes.

3.2 Nonlinear problem

Next we consider the nonlinear initial value problem

$$\dot{y}(t) = \sin(2\pi y(t)), \quad t \in (0, 1], \quad y(0) = \frac{1}{4}.$$

The analytic solution to this problem is

$$y(t) = \frac{1}{\pi} \arctan(e^{2\pi t}).$$

Let $R = 0.4$ and $S(y(t)) = y(t)$. The true QoI is

$$t_t = Q(y) = \min_{t \in [0, 1]} \arg(y(t) = 0.4) = \frac{\ln(\tan(0.4\pi))}{2\pi}.$$

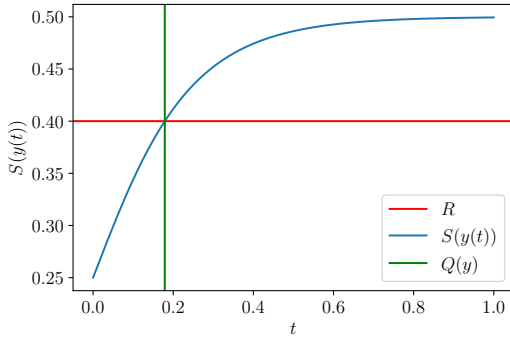
Here, the terms in (21) are

$$v = 1, \quad f(y, t) = \sin(2\pi y), \quad \nabla_y f(y, t) = 2\pi \cos(2\pi y),$$

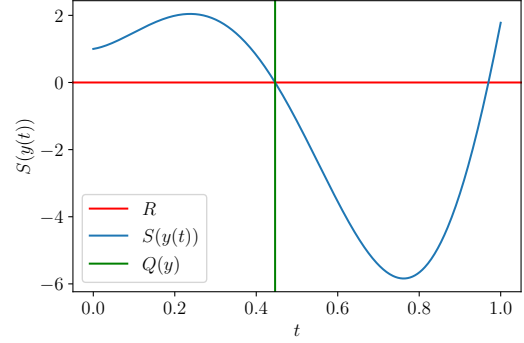
so the data needed for (22), (23), and (27) are

$$\psi_1 = -1, \quad \psi_2 = 2\pi \cos(2\pi R), \quad \psi_3 = 1.$$

Figure 4a shows the true values of the linear functional $S(y(t))$ as well as the event in question and the true QoI. The values in Tables 3 and 4 indicate that all three methods are fairly accurate. The two iterative methods again require more adjoint equations to be solved.



(a) Chosen value of R , true data $S(y(t))$, and true QoI for example in §3.2.



(b) Chosen value of R , true data $S(y(t))$, and true QoI for example in §3.3

Figure 4

Method	t_c	t_{LL}	t_L	t_R	e_Q	η	ρ_{eff}	n_{adj}
Taylor series	0.1790	—	—	—	-1.087e-04	-1.086e-04	1.000	2
Secant	0.1790	—	0.175	0.2	-1.087e-04	-1.087e-04	1.000	6
Inverse quad.	0.1790	0.15	0.175	0.2	-1.087e-04	-1.087e-04	1.000	6

Table 3: Results for §3.2 using the different methods on cG(1) solution with 40 elements.

Method	t_c	t_{LL}	t_L	t_R	e_Q	η	ρ_{eff}	n_{adj}
Taylor series	0.1810	–	–	–	-2.156e-03	-2.141e-03	1.007	2
Secant	0.1810	–	0.15	0.2	-2.156e-03	-2.144e-03	1.001	7
Inverse quad.	0.1810	0.1	0.15	0.2	-2.156e-03	-2.144e-03	1.001	7

Table 4: Results for §3.2 using the different methods on Crank-Nicolson solution with 21 nodes.

3.3 Linear system

We consider the two dimensional system $\dot{y} + A(t)y = 0$,

$$\begin{pmatrix} \dot{y}_1(t) \\ \dot{y}_2(t) \end{pmatrix} + \begin{pmatrix} 1 + 9 \cos^2(6t) - 6 \sin(12t) & -12 \cos^2(6t) - 9/2 \sin(12t) \\ 12 \sin^2(6t) - 9/2 \sin(12t) & 1 + 9 \sin^2(6t) + 6 \sin(12t) \end{pmatrix} \begin{pmatrix} y_1(t) \\ y_2(t) \end{pmatrix} = \begin{pmatrix} 0 \\ 0 \end{pmatrix}, \quad t \in (0, 1],$$

with initial conditions $y_1(0) = y_2(0) = 1$. The analytic solution to this problem is

$$\begin{pmatrix} y_1(t) \\ y_2(t) \end{pmatrix} = \begin{pmatrix} 3/5 \exp(2t)(\cos(6t) + 2 \sin(6t)) - 1/5 \exp(-13t)(\sin(6t) - 2 \cos(6t)) \\ 3/5 \exp(2t)(2 \cos(6t) - \sin(6t)) - 1/5 \exp(-13t)(\cos(6t) + 2 \sin(6t)) \end{pmatrix}.$$

Set $R = 0$ and $S(y(t)) = y_1(t)$ in order to analyze the first component. The true quantity of interest is

$$t_t := Q(y) = 0.446255366908554$$

The parameters needed for (21) are

$$v = (1, 0)^\top, \quad f(y, t) = -A(t)y, \quad \nabla_y f(y, t) = -A(t).$$

For (22), (23), and (27) the values needed are

$$\psi_1 = -(1, 0)^\top, \quad \psi_2 = (1 + 9 \cos^2(6t_c) - 6 \sin(12t_c), -12 \cos^2(6t_c) - \frac{9}{2} \sin(12t_c))^\top, \quad \psi_3 = (1, 0)^\top.$$

The true solution and QoI are shown in Figure 4b. Tables 5 and 6 show the results for cG(1) and Crank-Nicolson respectively. Again, all methods are accurate using either numerical method. The two iterative methods require many more adjoint problems to be solved than the Taylor series method without any increase in accuracy.

Method	t_c	t_{LL}	t_L	t_R	e_Q	η	ρ_{eff}	n_{adj}
Taylor series	0.4463	–	–	–	-1.323e-04	-1.322e-04	0.999	2
Secant method	0.4463	–	0.425	0.45	-1.323e-04	-1.323e-04	1.000	6
Inverse quad.	0.4463	0.4	0.425	0.45	-1.323e-04	-1.323e-04	1.000	8

Table 5: Results of the different methods on example in §3.3 using cG(1) with 40 elements.

Method	t_c	t_{LL}	t_L	t_R	e_Q	η	ρ_{eff}	n_{adj}
Taylor series	0.4462	–	–	–	2.675e-05	2.675e-05	1.000	2
Secant	0.4462	–	0.4	0.45	2.675e-05	2.675e-05	1.000	6
Inverse quad.	0.4462	0.35	0.4	0.45	2.675e-05	2.675e-05	1.000	8

Table 6: Results of the different methods on example in §3.3 using Crank-Nicolson with 21 nodes.

3.4 Harmonic oscillator

Consider the harmonic oscillator

$$\ddot{\omega} = -\frac{k}{m}\omega - \frac{c}{m}\dot{\omega} + \frac{F_0}{m}\cos(\gamma t + \theta_d), \quad t \in (0, 2], \quad \omega(0) = 5, \quad \dot{\omega}(0) = 0.$$

with

$$k = 50, \quad m = 0.25, \quad c = 1, \quad F_0 = 50, \quad \theta_d = 0, \quad \gamma = 10.$$

Rewriting as a system of first-order ODEs, $\dot{y} + Ay = h(t)$, gives

$$\begin{pmatrix} \dot{y}_1(t) \\ \dot{y}_2(t) \end{pmatrix} + \begin{pmatrix} 0 & -1 \\ 200 & 4 \end{pmatrix} \begin{pmatrix} y_1(t) \\ y_2(t) \end{pmatrix} = \begin{pmatrix} 0 \\ 200 \cos(10t) \end{pmatrix}.$$

Set $R = 0$ and $S(y(t)) = y_1(t)$ in order to observe when the oscillator first reaches the origin. The true solution in [5] is used to determine

$$t_t := Q(\omega) = 0.14034864129073557.$$

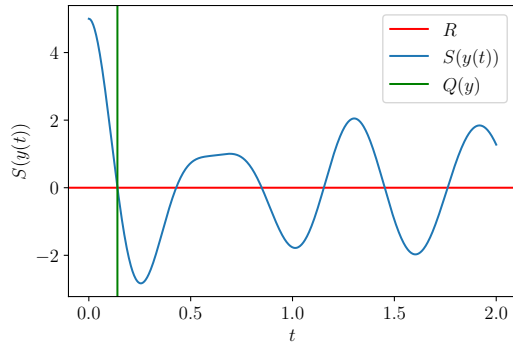
Here for (21), the values needed are

$$v = (1, 0)^\top, \quad f(y, t) = -Ay + h(t), \quad \nabla_y f(y, t) = -A.$$

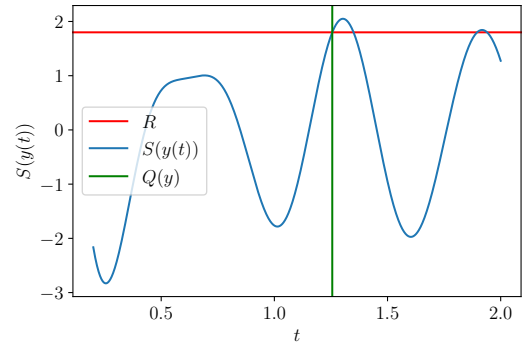
To compute (22), (23), and (27), let

$$\psi_1 = -(1, 0)^\top, \quad \psi_2 = (0, 1)^\top, \quad \psi_3 = (1, 0)^\top.$$

The true data $S(y(t))$ and QoI are given in Figure 5a and the results using cG(1) and Crank-Nicolson method are provided in Tables 7 and 8 respectively. All methods using either numerical method give effectivity ratios close to one. The two iterative methods require more adjoint problems to be solved than the Taylor series estimate, but they do lead to a slightly more accurate error estimate.



(a) Chosen value of R , true data $S(y(t))$, and true QoI $Q(y)$ for example 3.4



(b) Chosen value of R , true data $S(y(t))$, and true QoI $Q(y)$ for example in §3.4.1

Figure 5

3.4.1 Harmonic Oscillator: Effect of choice of interval

We consider the same equation and function as in §3.4, except over the time interval $t \in (0.2, 2]$ and with $R = 1.8$.

Method	t_c	t_{LL}	t_L	t_R	e_Q	η	ρ_{eff}	n_{adj}
Taylor series	0.1447	–	–	–	-4.440e-03	-4.449e-03	1.011	2
Secant method	0.1447	–	0.1	0.15	-4.440e-03	-4.440e-03	1.000	7
Inverse quad.	0.1447	0.05	0.1	0.15	-4.440e-03	-4.440e-03	1.000	8

Table 7: Results of the different methods on the example in §3.4 using cG(1) with 40 elements.

Method	t_c	t_{LL}	t_L	t_R	e_Q	η	ρ_{eff}	n_{adj}
Taylor series	0.1575	–	–	–	-1.715e-02	-1.816e-02	1.059	2
Secant method	0.1575	–	0.1	0.2	-1.715e-02	-1.715e-02	0.999	8
Inverse quad.	0.1575	0.0	0.1	0.2	-1.715e-02	-1.715e-02	0.999	10

Table 8: Results of the different methods on the example in §3.4 using Crank-Nicolson with 21 nodes.

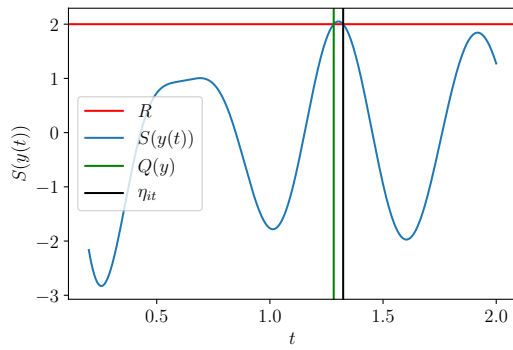
Applying the secant method to the true solution results in the true QoI,

$$t_t = 1.2558594599461572.$$

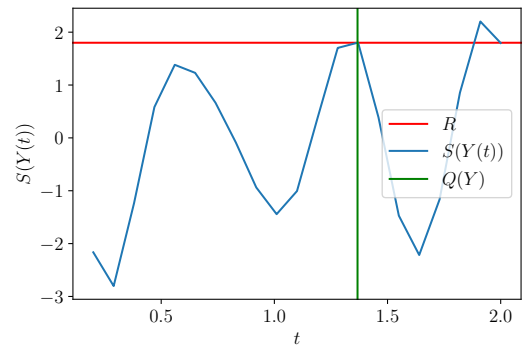
Since this problem has the same ODE and functional S as in §3.4, the parameters and steps laid out in that section can be used to obtain the error estimates.

The true functional and QoI are shown in Figure 5b and the results when using the different methods in Tables 9 and 10. The Taylor series method is slightly less accurate compared to the iterative methods when using the cG(1) method. This is due to the size of the second derivative of the functional near the event, leading to a larger absolute value of the remainder in (16). Since the error estimate (21) neglects this remainder, if its absolute value is too large the estimate will not be accurate. Examples in §3.4.2 take a further look into this effect.

Both the Taylor series and iterative methods are poor for the Crank-Nicolson method. This is due to the low accuracy of the numerical solution as illustrated in Figure 6b. This inaccuracy of the the Taylor series estimate is discussed in Remark 1. The root-finding methods are converging to the *second* time the event occurs (which is 1.3237), rather than the first, because of the proximity of the second time value to the numerical QoI, see Figure 6a.



(a) Figure detailing issue with iterative methods in §3.4.1 and §3.4.2 when the numerical solution is not accurate near the event. The iterative methods result in $t^* = \eta_{it}$, which is the second occurrence of the event rather than the first. This figure specifically details the case when $R = 2$.



(b) Numerical values for example in §3.4.1 when using Crank-Nicolson method with 21 nodes.

Figure 6

Method	t_c	t_{LL}	t_L	t_R	e_Q	η	ρ_{eff}	n_{adj}
Taylor series	1.2637	—	—	—	-7.887e-03	-8.623e-03	1.093	2
Secant	1.2637	—	1.235	1.37	-7.887e-03	-7.887e-03	0.999	8
Inverse quad.	1.2637	1.19	1.235	1.37	-7.887e-03	-7.887e-03	0.999	9

Table 9: Results of the different methods on example in §3.4.1 using cG(1) with 40 elements.

Method	t_c	t_{LL}	t_L	t_R	e_Q	η	ρ_{eff}	n_{adj}
Taylor series	1.3674	—	—	—	-1.116e-01	-1.542e-02	0.138	2
Secant method	1.3674	—	1.28	1.37	-1.116e-01	-1.746e-02	0.156	8
Inverse quad.	1.3674	1.19	1.28	1.37	-1.116e-01	-1.746e-02	0.156	10

Table 10: Results of the different methods on example in §3.4.1 using Crank-Nicolson with 21 nodes.

3.4.2 Harmonic oscillator: Effect of choice of R

Again consider the harmonic oscillator of §3.4.1, and estimate the error of the QoI (2) with several different values of R , increasing R until it is very close to the maximum of the true data. The maximum value of the true data is approximately 2.05015. Results are provided in Tables 11, 12 and 13 for increasingly fine finite element meshes. The Tables contain the effectivity ratios, ρ_{eff} , for each method and each value of R .

Notice that the iterative methods are more reliant on the accuracy of the numerical solution. As the number of finite elements used to solve the ODE increases, the two iterative methods eventually recover their accuracy even when the threshold value is very close to an extremum. For the cases where the iterative methods are inaccurate, note that the root-finding schemes do *not* converge to the true QoI. Instead, the convergence is to the *second* occurrence of the event rather than the first (see Figure 6a). In some cases, the iterative methods fail to converge. This happens when a root-finding iteration falls outside of the domain of the IVP (1), that is if the guess to the root at the n th iteration is x_n , then either $x_n < 0$ or $x_n > T$. Our estimate derived from Taylor's theorem is generally more accurate for the less accurate solutions.

Even when using a more accurate numerical solution, this method is inaccurate when the curvature of the S as a function of t is large near the threshold value. The inaccuracy happens because the remainder $\mathcal{R}_1(t, t_c)$, given by (2), contains the second derivative (or curvature) of S with respect to t . As the threshold value R moves closer to the local maximum of the curve, this derivative grows and hence $\mathcal{R}_1(t, t_c)$ also grows. Since (21) neglects $\mathcal{R}_1(t, t_c)$, the increasing absolute value of the second derivative leads to an inaccurate estimate. The iterative methods do not depend on the values of the second derivative of the solution thus those methods are able to produce accurate error estimates as long as the numerical solution is accurate enough near the event.

Method	R=1.95	R=2.0	R=2.01	R=2.02	R=2.03	R=2.04	R=2.05
Taylor series	1.061	1.095	1.251	1.603	3.470	-1.137	0.427
Secant method	0.999	-11.305	-4.952	-2.650	-1.405	1.000	fail
Inverse quad.	0.999	-11.305	-4.952	-2.650	-1.405	fail	fail

Table 11: Results of the different methods for varying values of R on example in §3.4 using cG(1) with 40 elements.

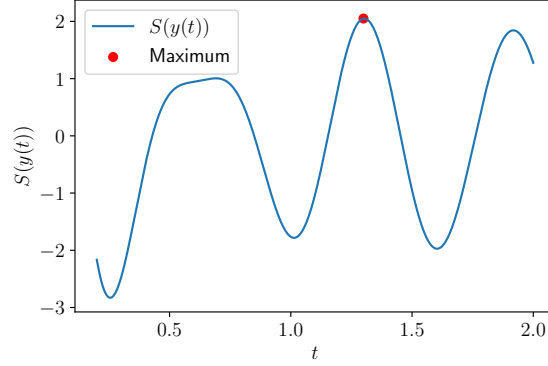


Figure 7: True data for example in §3.4.1, showing max value of ≈ 2.05015 .

Method	R=1.95	R=2.0	R=2.01	R=2.02	R=2.03	R=2.04	R=2.05
Taylor series	1.033	0.999	1.043	1.100	1.179	1.283	0.758
Secant	1.000	0.999	0.999	0.999	-6.545	-4.520	3.133
Inverse quad.	1.000	0.999	0.999	0.999	-6.545	-4.520	3.133

Table 12: Results of the different methods for varying values of R on example in §3.4 using cG(1) with 60 elements.

Method	R=1.95	R=2.0	R=2.01	R=2.02	R=2.03	R=2.04	R=2.05
Taylor series	1.017	1.001	1.019	1.100	1.039	0.998	0.588
Secant	0.999	0.999	0.999	1.000	0.999	0.999	0.999
Inverse quad.	0.999	0.999	0.999	1.000	0.999	0.999	0.999

Table 13: Results of the different methods for varying values of R on example in §3.4 using cG(1) with 100 elements.

3.5 One dimensional heat equation

We consider the one dimensional heat equation with boundary and initial conditions

$$\begin{aligned}
u_t(x, t) &= u_{xx}(x, t) + \sin(\pi x) \cos(2\pi t), \quad (x, t) \in (0, 1) \times (0, 1], \\
u(x, 0) &= 0, \quad x \in (0, 1), \\
u(0, t) &= 0, \quad u(1, t) = 0, \quad t \in (0, 1].
\end{aligned}$$

This section analyzes the system of ordinary differential equations that arises from a spatial discretization of (3.5) using a central-difference method. In particular using a uniform partition of the spatial interval $[0, 1]$ with 22 nodes:

$$\{0 = x_0 < x_1 < \cdots < x_{21} = 1\}.$$

Since boundary values are specified, this semi-discretization leads to a system of 20 first-order ODEs of the form $\dot{y}(t) = Ay(t) + k(t)$, where $h = \frac{1}{21}$ and

$$A = \frac{1}{h^2} \begin{pmatrix} -2 & 1 & 0 & \cdots & \cdots & 0 \\ 1 & -2 & 1 & 0 & \cdots & 0 \\ 0 & 1 & -2 & 1 & \cdots & 0 \\ \vdots & & \ddots & \ddots & \ddots & \vdots \\ 0 & \cdots & 0 & 1 & -2 & 1 \\ 0 & \cdots & \cdots & 0 & 1 & -2 \end{pmatrix}, \quad k(t) = \begin{pmatrix} \sin(\pi x_1) \cos(2\pi t) \\ \sin(\pi x_2) \cos(2\pi t) \\ \sin(\pi x_3) \cos(2\pi t) \\ \vdots \\ \sin(\pi x_{19}) \cos(2\pi t) \\ \sin(\pi x_{20}) \cos(2\pi t) \end{pmatrix}$$

Since this problem will only analyze the semi-discrete system and not the full PDE, a reference solution is obtained using an accurate time-integrator (SciPy's `solve_ivp`) using an absolute tolerance of 10^{-15} . Let $R = 0.33$ and $S(y(t)) = \frac{1}{20} \sum_{i=1}^{20} y_i(t)$ in order to analyze the discrete average of the solution over the spatial domain at a time t . This library function also has the capability of tracking when specified events occur, which is used to obtain a reference for the true QoI,

$$t_t = 0.5834435609935992.$$

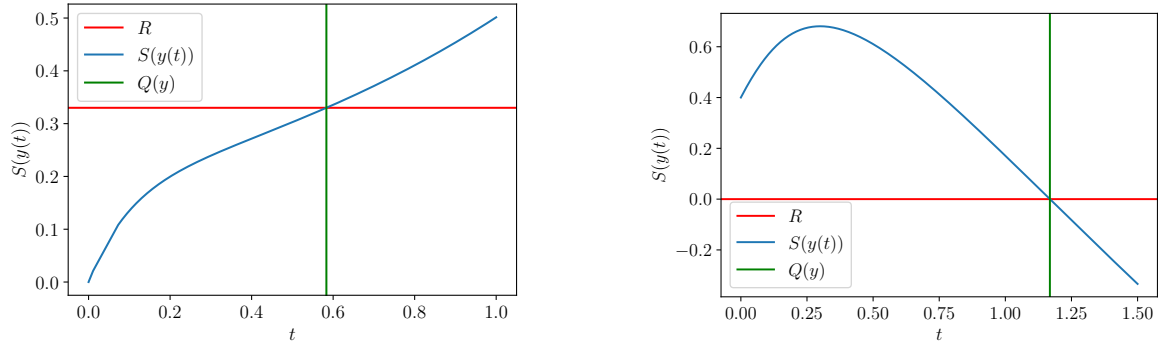
For this problem, the parameters in (21) are

$$v = \frac{1}{20}(1, 1, \dots, 1)^\top, \quad f(y, t) = Ay + k(t), \quad \nabla_y f(y, t) = A.$$

For (22), (23), and (27), set

$$\psi_1 = -\frac{1}{20}(1, 1, \dots, 1)^\top, \quad \psi_2 = \frac{1}{20h^2}(-1, 0, \dots, 0, -1)^\top, \quad \psi_3 = \frac{1}{20}(1, 1, \dots, 1)^\top.$$

The true solution and QoI are shown in Figure 8a and the results when using cG(1) or Crank-Nicolson methods are shown in Tables 14 and 15 respectively. All methods are accurate using either numerical method. The two iterative methods require more adjoint problems to be solved than the Taylor series estimate without any noticeable increase in accuracy.



(a) Chosen value of R , true data $S(y(t))$, and true QoI for example in §3.5.

(b) Chosen value of R , true data $S(y(t))$, and true QoI for example in §3.6.

Figure 8

Method	t_c	t_{LL}	t_L	t_R	e_Q	η	ρ_{eff}	n_{adj}
Taylor series	0.5834	—	—	—	6.157e-05	6.151e-05	0.999	2
Secant	0.5834	—	0.575	0.6	6.157e-05	6.150e-05	0.999	6
Inverse quad.	0.5834	0.55	0.575	0.6	6.157e-05	6.150e-05	0.999	7

Table 14: Results of the different methods on the example in §3.5 using cG(1) with 40 elements.

Method	t_c	t_{LL}	t_L	t_R	e_Q	η	ρ_{eff}	n_{adj}
Taylor series	0.5830	—	—	—	4.457e-04	4.457e-04	1.000	2
Secant	0.5830	—	0.55	0.6	4.457e-04	4.456e-04	0.999	6
Inverse quad.	0.5830	0.5	0.55	0.6	4.457e-04	4.456e-04	0.999	7

Table 15: Results of the different methods on the example in §3.5 using Crank-Nicolson with 21 nodes.

3.6 Two body problem

We consider the two body problem

$$\left. \begin{aligned} \dot{y}_1 &= y_3, \\ \dot{y}_2 &= y_4, \\ \dot{y}_3 &= \frac{-y_1}{(y_1^2 + y_2^2)^{3/2}}, \\ \dot{y}_4 &= \frac{-y_2}{(y_1^2 + y_2^2)^{3/2}}, \end{aligned} \right\} \quad t \in (0, 1.5], \quad y(0) = (0.4, 0, 0, 2.0)^\top,$$

which models a small body orbiting a much larger body in two dimensions. Here y_1, y_2 are the spatial coordinates of the orbiting body relative to the larger body, and y_3, y_4 are the respective velocities. The initial conditions are chosen so that the analytic solution is [25]

$$y = \left(\cos(\tau) - 0.6, 0.8 \sin(\tau), \frac{-\sin(\tau)}{1 - 0.6 \cos(\tau)}, \frac{0.8 \cos(\tau)}{1 - 0.6 \cos(\tau)} \right)^\top,$$

where τ solves $\tau - 0.6 \sin(\tau) = t$. Let $R = 0$ and $S(y(t)) = y_1(t) + y_2(t)$. The true QoI can be found exactly:

$$t_t = Q(y) = \cos^{-1}((15 - 16\sqrt{2})/41) - 0.6 \sin(\cos^{-1}((15 - 16\sqrt{2})/41)).$$

The values needed to compute (21) are

$$v = (1, 1, 0, 0)^\top, \quad f(y, t) = \left(y_3, y_4, \frac{-y_1}{(y_1^2 + y_2^2)^{3/2}}, \frac{-y_2}{(y_1^2 + y_2^2)^{3/2}} \right)^\top,$$

and

$$\nabla_y f(y, t) = \begin{pmatrix} 0 & 0 & 1 & 0 \\ 0 & 0 & 0 & 1 \\ \frac{2y_1^2 - y_2}{(y_1^2 + y_2^2)^{5/2}} & \frac{3y_1 y_2}{(y_1^2 + y_2^2)^{5/2}} & 0 & 0 \\ \frac{3y_1 y_2}{(y_1^2 + y_2^2)^{5/2}} & \frac{2y_1^2 - y_2}{(y_1^2 + y_2^2)^{5/2}} & 0 & 0 \end{pmatrix}.$$

For (22), (23), and (27), the data needed are

$$\psi_1 = (-1, -1, 0, 0)^\top, \quad \psi_2 = (0, 0, 1, 1)^\top, \quad \psi_3 = (1, 1, 0, 0)^\top.$$

The true data $S(y(t))$ and QoI are shown in Figure 8b and the results using the cG(1) and Crank-Nicolson method appear in Tables 16 and 17 respectively. All methods have larger error than in other examples so far. This is likely do to the non-linear nature of (3.6). However the error estimates are still accurate using either numerical method; each with an effectivity ratio close to one.

Method	t_c	t_{LL}	t_L	t_R	e_Q	η	ρ_{eff}	n_{adj}
Taylor series	1.1601	—	—	—	8.262e-03	8.287e-03	1.003	2
Secant method	1.1601	—	1.125	1.1625	8.262e-03	8.287e-03	1.003	5
Inverse quad.	1.1601	1.0875	1.125	1.1625	8.262e-03	8.287e-03	1.003	6

Table 16: Results of the different methods on the example in §3.6 using cG(1) with 40 elements.

Method	t_c	t_{LL}	t_L	t_R	e_Q	η	ρ_{eff}	n_{adj}
Taylor series	1.2091	—	—	—	-4.068e-02	-4.078e-02	1.002	2
Secant	1.2091	—	1.2	1.275	-4.068e-02	-4.077e-02	1.002	5
Inverse quad.	1.2091	1.125	1.2	1.275	-4.068e-02	-4.077e-02	1.002	6

Table 17: Results of the different methods on the example in §3.6 using Crank-Nicolson with 21 nodes.

3.7 Logistic Equation

Consider the Logistic equation

$$\dot{P} = kP \left(1 - \frac{P}{K} \right), \quad t \in (0, 20], \quad P(0) = \frac{1}{2}, \quad (38)$$

where $k = 0.25$ and $K = 1$. The analytic solution is,

$$P(t) = \frac{K P(0)}{P(0) + (K - P(0))e^{-kt}} = \frac{1}{1 + 3e^{-0.25t}}. \quad (39)$$

Let $S(P(t)) = P(t)$ and consider several threshold values, $R \in \{0.55, 0.8, 0.9, 0.95, 0.98, 0.99, 0.995\}$. The values needed for (21) are

$$v = 1, \quad f(y, t) = ky \left(1 - \frac{y}{K} \right), \quad \nabla_y f(y, t) = k - \frac{2k}{K}y,$$

so the data needed for (22), (23), and (27) are

$$\psi_1 = -1, \quad \psi_2 = k - \frac{2k}{K}R, \quad \psi_3 = 1.$$

The numerical solution is computed using the cG(1) method with five elements. Figure 9 shows the true functional and QoI for a chosen threshold value. Table 18 shows the true error in the QoI and the effectivity ratio for each method as the threshold value increases. We see that as the error in the QoI increases, the Taylor series method loses accuracy but the iterative methods are accurate even when the true error is greater than one. The iterative methods are accurate because the root finding techniques are able to find the correct root. This is due to the lack of any oscillations in the functional and so there are no other, incorrect roots as was the case in §3.4.1.

	R=0.55	R=0.8	R=0.9	R=0.94	R=0.98	R=0.99	R=0.995
e_Q	-0.090	-0.117	-0.166	0.194	0.829	0.610	1.513
Taylor series	1.001	1.021	1.041	0.957	0.902	0.919	0.830
Secant	0.999	0.987	0.977	1.023	1.007	1.011	1.005
Inverse quad.	0.999	0.987	0.977	1.023	1.007	1.011	1.005

Table 18: Error in QoI and effectivity ratio of the different methods for varying values of R on example in §3.7 using cG(1) with 5 elements.

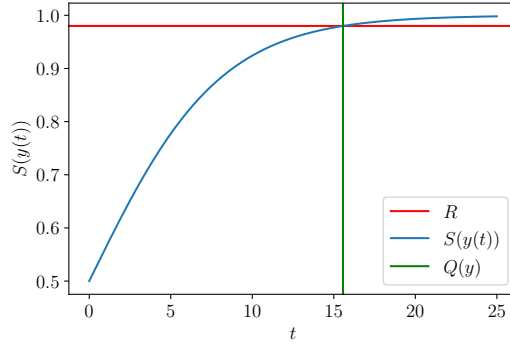


Figure 9: True values of functional and QoI for example in §3.7, when $R = 0.94$

3.8 Conclusions for deterministic examples

We see that both the Taylor series and the root-finding approaches lead to accurate error estimates in most cases. Some limitations of these methods were revealed in §3.4.1 and §3.4.2. The poor results in §3.4.1 are caused by the use of a low accuracy solution and the fact that computed QoI was closer to the second time the threshold value was crossed than the first. In section 3.4.2, specifically Tables 11, 12 and 13, we see that the issue that arose in §3.4.1 can be remedied by using a numerical solution that is more accurate near the QoI. Although another issue is revealed in the final column of Table 13, where the Taylor series approach gives poor results even though the numerical solution is quite accurate. In that instance the poor result is likely due to the remainder in (16) being too large to neglect. The example in §3.7 shows that the Taylor series approach may not be accurate if the error in the QoI is large, but the iterative methods are accurate as long as the root finding technique find the correct root.

4 Numerical examples for error in the CDF of the non-standard QoI

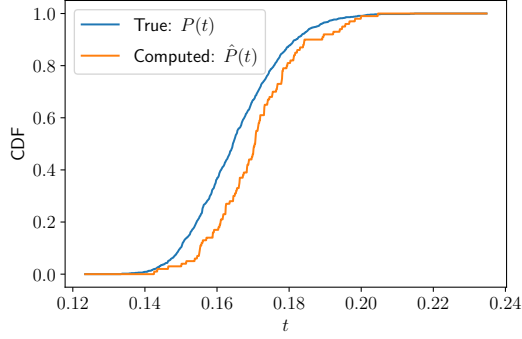
The techniques outlined in §2.5 are applied to some examples below. The error bound (35) relies on accurate error estimates for the non-standard QoI. In the numerical examples, the estimates for the error in each sample value had an effectivity ratio close to one.

4.1 Harmonic oscillator

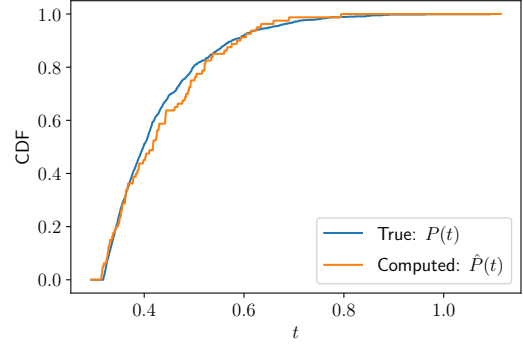
Reconsider the harmonic oscillator from §3.4 this time with parameters k and m as random variables:

$$\begin{pmatrix} \dot{y}_1(t) \\ \dot{y}_2(t) \end{pmatrix} + \begin{pmatrix} 0 & -1 \\ k/m & 1/m \end{pmatrix} \begin{pmatrix} y_1(t) \\ y_2(t) \end{pmatrix} = \begin{pmatrix} 0 \\ 50/m * \cos(10t) \end{pmatrix}, \quad t \in (0, 2],$$

with initial conditions $(y_1(0), y_2(0)) = (5, 0)$. Let k have a normal distribution with mean 50 and variance 5 and m have a normal distribution with mean 0.25 and variance 0.02. For the QoI, set choose $R = -1$ and $S(y(t)) = y_1(t)$. With $\varepsilon = 0.5$ in (35), the nominal CDF (33) is computed using the true solution given in [5] with 1000 samples. The numerical solution is obtained using cG(1) with 40 elements and the approximate CDF (32) is computed with $N = 100$ samples. The error here is most affected by stochastic sources. This is to be expected from this example, given that an accurate numerical solution is used and the fact that there are two sources of stochastic error. The computed bound is indeed larger than the actual error in the distribution. Both the bound and the error peak near the inflection point of the CDF, with the error bound being about five times larger than the true error. This is consistent with results shown elsewhere, see [13].

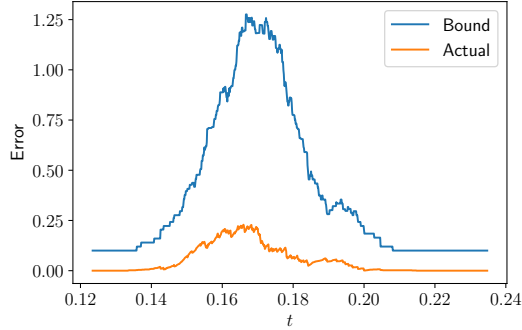


(a) Nominal CDF using 1000 samples and computed CDF using 100 samples for example in §4.1.

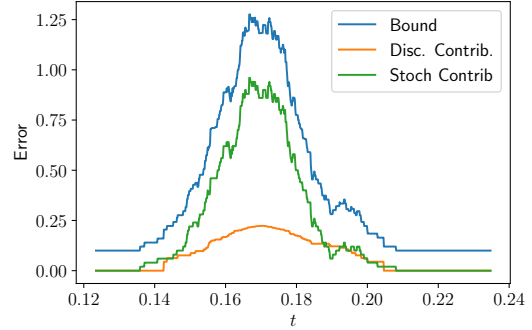


(b) Comparing nominal CDF using 1000 samples to computed CDF using 80 samples for example in §4.2.

Figure 10



(a) Comparing computed error bound (35) to true error for the problem in §4.1 when using 1000 samples for the nominal CDF and 100 samples for the numerical CDF.



(b) Breaking the error bound into stochastic and discretization contributions for the problem in §4.1 when using 100 samples. The stochastic and discretization contributions are computed as the first and second terms of (35), respectively.

Figure 11: Error bound for example in §4.1.

4.2 Lorenz System

Consider the Lorenz system (3). Again let $\sigma = 10$, $r = 28$, and $b = \frac{8}{3}$. For the QoI (2), set $R = 3$ and $S(y(t)) = y_1(t)$. A reference solution and QoI are obtained using an accurate time-integrator (SciPy's `solve_ivp` with event tracker) with an absolute tolerance of 10^{-15} and a relative tolerance of 10^{-8} . This time, the numerical solution is computed using the `cG(1)` method with 30 elements.

The values needed for equation (21) are

$$v = (1, 0, 0)^\top, f(y, t) = (\sigma(y_2 - y_1), ry_1 - y_2 - y_1y_3, y_1y_2 - by_3)^\top,$$

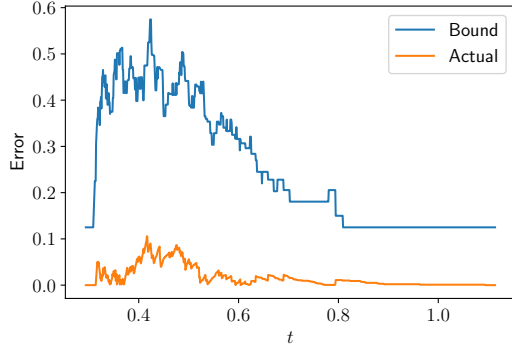
and

$$\nabla_y f(y, t) = \begin{pmatrix} \sigma & -\sigma & 0 \\ r - y_3 & -1 & -y_1 \\ -y_2 & y_1 & -b \end{pmatrix}.$$

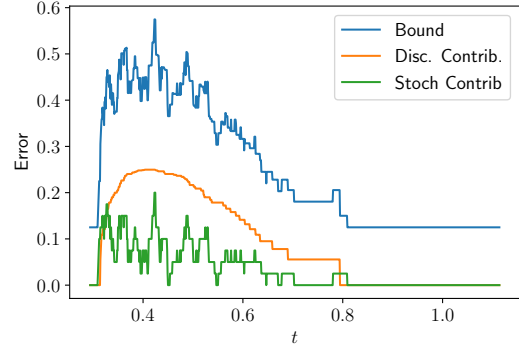
hence, for (22), (23), and (27) the data are

$$\psi_1 = (-1, 0, 0)^\top, \psi_2 = (-\sigma, \sigma, 0)^\top, \psi_3 = (1, 0, 0)^\top.$$

The bound (35) is computed with $\varepsilon = 0.05$. The Figure 10b compares the numerical CDF computed using 80 samples to the nominal CDF using 1000 samples. Figure 12 shows the discretization and stochastic contributions to the calculated error bound. For this example, the discretization is the larger contributor to the error in the CDF, which is likely due to the chaotic nature of the system. As in §4.1 the error bound is roughly five times the true error at its peak.



(a) Comparing error bound (35) to true error for example in §4.2 when using 1000 samples for the nominal CDF and 80 samples for the numerical CDF.



(b) Showing the stochastic and discretization contributions to the error bound for the example in §4.2 when using 100 samples. The stochastic contribution is computed as the first term of (35), while the second term gives the discretization contribution.

Figure 12

5 Conclusions

We develop two different classes of accurate *a posteriori* error estimates for a QoI that cannot be expressed as a bounded functional of the solution, namely the first time when a given functional S of the solution achieves a specific value. The first method is based on Taylor's Theorem and is accurate whenever the numerical solution is sufficiently accurate and the curvature of the functional S is not too large. Moreover this method is cost effective, requiring the solution of only two adjoint problems. The second method is based on standard root-finding techniques and are accurate provided the numerical solution is accurate near the event of interest. These estimates however are more costly, requiring an adjoint solution per iteration of the root-finding algorithm. Both methods can be used as a basis for determining the deterministic contribution to an error bound on a CDF of the functional when one or more of the parameters governing the system of differential equations are random variables.

References

- [1] M. Ainsworth and T. Oden. *A posteriori error estimation in finite element analysis*. John Wiley-Teubner, 2000.
- [2] Tom M. Apostol. *Calculus*, volume 1. Wiley, 2nd edition, 1967.
- [3] Tom M. Apostol. *Calculus*, volume 2. Wiley, 2nd edition, 1969.
- [4] W. Bangerth and R. Rannacher. *Adaptive Finite Element Methods for Differential Equations*. Birkhauser Verlag, 2003.
- [5] V. Barger and M. Olsson. *Classical Mechanics, A Modern Perspective*. McGraw-Hill, New York, 1973.
- [6] T. J. Barth. *A posteriori Error Estimation and Mesh Adaptivity for Finite Volume and Finite Element Methods*, volume 41 of *Lecture Notes in Computational Science and Engineering*. Springer, New York, 2004.
- [7] R. Becker and R. Rannacher. An optimal control approach to *a posteriori* error estimation in finite element methods. *Acta Numerica*, pages 1–102, 2001.
- [8] Yang Cao and Linda Petzold. A posteriori error estimation and global error control for ordinary differential equations by the adjoint method. *SIAM Journal on Scientific Computing*, 26(2):359–374, 2004.
- [9] V. Carey, D. Estep, and S. Tavener. A posteriori analysis and adaptive error control for multiscale operator decomposition solution of elliptic systems I: Triangular systems. *SIAM Journal on Numerical Analysis*, 47(1):740–761, 2008.
- [10] J. H. Chaudhry, D. Estep, V. Ginting, and S.J. Tavener. A posteriori analysis for iterative solvers for nonautonomous evolution problems. *SIAM/ASA J. Uncertainty Quantification*, 3(1):434–459, 2015.
- [11] Jehanzeb Chaudhry, Don Estep, and Simon Tavener. A posteriori error analysis for Schwarz overlapping domain decomposition methods. *arXiv e-prints*, page arXiv:1907.01139, Jul 2019.
- [12] Jehanzeb H Chaudhry. A Posteriori Analysis and Efficient Refinement Strategies for the Poisson–Boltzmann Equation. *SIAM Journal on Scientific Computing*, 40(4):A2519–A2542, 2018.
- [13] Jehanzeb H. Chaudhry, Nathaniel Burch, and Donald Estep. Efficient distribution estimation and uncertainty quantification for elliptic problems on domains with stochastic boundaries, 2018.

- [14] Jehanzeb H. Chaudhry, J.B. Collins, and John N. Shadid. A posteriori error estimation for multi-stage runge-kutta imex schemes. *Applied Numerical Mathematics*, 117:36–49, Jul 2017.
- [15] Jehanzeb H. Chaudhry, Donald Estep, Victor Ginting, John N. Shadid, and Simon Tavener. A posteriori error analysis of IMEX multi-step time integration methods for advection-diffusion-reaction equations. *To be published in CMAME*, 2014.
- [16] Jehanzeb H Chaudhry, Donald Estep, Victor Ginting, John N Shadid, and Simon Tavener. A posteriori error analysis of imex multi-step time integration methods for advection–diffusion–reaction equations. *Computer Methods in Applied Mechanics and Engineering*, 285:730–751, 2015.
- [17] Jehanzeb Hameed Chaudhry, Don Estep, Simon Tavener, Varis Carey, and Jeff Sandelin. A posteriori error analysis of two-stage computation methods with application to efficient discretization and the Parareal algorithm. *SIAM Journal on Numerical Analysis*, 54(5):2974–3002, 2016.
- [18] J.H. Chaudhry, D. Estep, V. Ginting, and S.J. Tavener. A posteriori analysis of an iterative multi-discretization method for reaction-diffusion systems. *Computer Methods in Applied Mechanics and Engineering*, 267:1–22, 2013.
- [19] J.H. Chaudhry, J.N. Shadid, and T. Wildey. A posteriori analysis of an IMEX entropy-viscosity formulation for hyperbolic conservation laws with dissipation. *Applied Numerical Mathematics*, 135, 2019.
- [20] J. H. Chaudry, D. Estep, V. Ginting, and S. Tavener. A posteriori analysis for iterative solvers for non-autonomous evolution problems. *SIAM Journal on Uncertainty Quantification*, 3, 2015.
- [21] J Collins, D Estep, and S Tavener. A posteriori error analysis for finite element methods with projection operators as applied to explicit time integration techniques. *BIT Numerical Mathematics*, 2014. DOI 10.1007/s10543-014-0534-9.
- [22] J. B. Collins, D. Estep, and S. Tavener. A posteriori error analysis for finite element methods with projection operators as applied to explicit time integration techniques. *BIT Numerical Mathematics*, 55(4):1017–1042, 2015.
- [23] James B Collins, Don Estep, and Simon Tavener. A posteriori error estimation for the lax–wendroff finite difference scheme. *Journal of Computational and Applied Mathematics*, 263:299–311, 2014.
- [24] JB Collins, Don Estep, and Simon Tavener. A posteriori error estimation for the Lax–Wendroff finite difference scheme. *Journal of Computational and Applied Mathematics*, 263:299–311, 2014.
- [25] Joseph B. Collins, Donald Estep, and Simon Tavener. A posteriori error analysis for finite element methods with projection operators as applied to explicit time integration techniques. *BIT Numerical Mathematics*, 55:1017–1042, 2015.
- [26] M. Delfour, W. Hager, and F. Trochu. Discontinuous Galerkin methods for ordinary differential equations. *Math. Comp.*, 36(154):455–473, 1981.
- [27] M. C. Delfour and F. Dubeau. Discontinuous polynomial approximations in the theory of one-step, hybrid and multistep methods for nonlinear ordinary differential equations. *Math. Comp.*, 47(175):169–189, S1–S8, 1986. With a supplement.
- [28] James F. Epperson. *An Introduction to Numerical Methods and Analysis*. Wiley-Interscience, 2007.
- [29] K. Eriksson, D. Estep, P. Hansbo, and C. Johnson. Introduction to adaptive methods for differential equations. In *Acta Numerica, 1995*, Acta Numerica, pages 105–158. Cambridge Univ. Press, Cambridge, 1995.

- [30] K. Eriksson, C. Johnson, and A. Logg. Explicit time-stepping for stiff ODEs. *SIAM Journal on Scientific Computing*, 25(4):1142–1157, 2004.
- [31] D. Estep. *A posteriori* error bounds and global error control for approximation of ordinary differential equations. *SIAM J. Numer. Anal.*, 32(1):1–48, 1995.
- [32] D. Estep. A short course on duality, adjoint operators, greens functions, and a posteriori error analysis. Unpublished, 2004.
- [33] D. Estep. Error estimates for multiscale operator decomposition for multiphysics models. In J. Fish, editor, *Multiscale methods: bridging the scales in science and engineering*. Oxford University Press, USA, 2009.
- [34] D. Estep, V. Ginting, and S. Tavener. A posteriori analysis of a multirate numerical method for ordinary differential equations. *Computer Methods in Applied Mechanics and Engineering*, 223:10–27, 2012.
- [35] D. Estep, M. Holst, and D. Mikulencak. Accounting for stability: a posteriori error estimates based on residuals and variational analysis. volume 18, pages 15–30. 2002.
- [36] D. Estep, M. Larson, and R. Williams. Estimating the error of numerical solutions of systems of reaction-diffusion equations. *Memoirs of the American Mathematical Society*, 696, 07 2000.
- [37] D. Estep, A. Målqvist, and S. Tavener. Nonparametric density estimation for randomly perturbed elliptic problems I: Computational methods, a posteriori analysis, and adaptive error control. *SIAM Journal on Scientific Computing*, 31(4):2935–2959, 2009.
- [38] D. Estep, A. Målqvist, and S. Tavener. Nonparametric density estimation for randomly perturbed elliptic problems II: Applications and adaptive modeling. *International Journal for Numerical Methods in Engineering*, 80(6-7), 2009.
- [39] Donald Estep, M. Larson, and R. Williams. Estimating the error of numerical solutions of systems of reaction-diffusion equations. *Memoirs of the American Mathematical Society*, 146(696), 2000.
- [40] Walter Gautschi. *Numerical Analysis*. Birkhäuser, 2011.
- [41] A. Johansson, J.H. Chaudhry, V. Carey, D. Estep, V. Ginting, M. Larson, and S.J. Tavener. Adaptive finite element solution of multiscale PDE–ODE systems. *Computer Methods in Applied Mechanics and Engineering*, 287:150–171, 2015.
- [42] Anders Logg. Multi-adaptive time integration. *Appl. Numer. Math.*, 48(3-4):339–354, mar 2004.

A Theorem 4

Theorem 4. *Numerical solutions obtained via the Crank-Nicolson finite difference scheme are nodally equivalent to solutions obtained using a cG(1) finite element method in which the integrals are evaluated with the trapezoidal rule.*

Proof. The cG(1) formulation over a sub-interval (t_n, t_{n+1}) , with the constant test function $v(t) = 1$ is

$$\int_{t_n}^{t_{n+1}} \dot{y} \, dt = \int_{t_n}^{t_{n+1}} f(y, t) \, dt. \quad (40)$$

Where by the fundamental theorem of calculus

$$\int_{t_n}^{t_{n+1}} \dot{y} \, dt = y(t_{n+1}) - y(t_n). \quad (41)$$

Using the trapezoidal quadrature rule, we obtain

$$\int_{t_n}^{t_{n+1}} f(y, t) \, dt \approx \frac{t_{n+1} - t_n}{2} (f(y(t_{n+1}), t_{n+1}) + f(y(t_n), t_n)). \quad (42)$$

Substituting (41) and (42) into (40) results in the Crank-Nicolson scheme. \square